

# Functionalization mediates heat transport in graphene nanoflakes

Haoxue Han,<sup>1,\*</sup> Yong Zhang,<sup>2</sup> Nan Wang,<sup>2</sup> Majid Kabiri Samani,<sup>2</sup> Zainelabideen Y. Mijbil,<sup>3</sup> Michael Edwards,<sup>2</sup> Yuxiang Ni,<sup>4</sup> Shiyun Xiong,<sup>5</sup> Kimmo Sääskilähti,<sup>6</sup> Hatf Sadeghi,<sup>3</sup> Murali Murugesan,<sup>2</sup> Yifeng Fu,<sup>2,7</sup> Lilei Ye,<sup>7</sup> Steven Bailey,<sup>3</sup> Yuriy A. Kosevich,<sup>1,8</sup> Colin J. Lambert,<sup>3,†</sup> Johan Liu,<sup>2,‡</sup> and Sebastian Volz<sup>1,§</sup>

<sup>1</sup>*Laboratoire EM2C, CNRS, CentraleSupélec, Université Paris-Saclay,  
Grande Voie des Vignes, 92295 Châtenay-Malabry, France*

<sup>2</sup>*Electronics Material and Systems Laboratory,  
Department of Microtechnology and Nanoscience,  
Chalmers University of Technology, SE-41296 Gothenburg, Sweden*

<sup>3</sup>*Quantum Technology Center, Physics Department,  
Lancaster University, LA1 4YB Lancaster, UK*

<sup>4</sup>*Department of Mechanical Engineering, University of Minnesota,  
111 Church Street SE, Minneapolis, MN 55455, USA*

<sup>5</sup>*Max Planck Institute for Polymer Research,  
Ackermannweg 10, D-55128 Mainz, Germany*

<sup>6</sup>*Department of Biomedical Engineering and Computational Science,  
Aalto University, FI-00076 Aalto, Finland*

<sup>7</sup>*SHT Smart High Tech AB, Ascherbergsgatan 46, 41133, Gothenburg, Sweden*

<sup>8</sup>*Semenov Institute of Chemical Physics, Russian Academy of Sciences,  
Kosygin str. 4, Moscow 119991, Russia*

(Dated: January 11, 2016)

## Abstract

Thermal management of high-power microelectronics by using graphene and few-layer graphene as excellent heat conductor has attracted tremendous attention. However, this high thermal conductivity undergoes severe degradations by contact with the substrate. Here we show experimentally that thermal management of a micro heater is substantially improved via introducing alternative heat-escaping channels into a graphene-based film covalently bonded to functionalized graphene oxide through amino-silane molecules. Using a resistance temperature probe for in situ monitoring we demonstrate that the temperature of the hotspots can be lowered by  $\sim 23^{\circ}\text{C}$  in chip operating at  $1300\text{ W cm}^{-2}$ , which corresponds to an order-of-magnitude increase in the device lifetime. Interface thermal resistance probed by pulsed photothermal reflectance measurements demonstrated an improved thermal coupling due to functionalization on the graphene-graphene oxide interface. Three functionalization polymers manifest distinct interfacial thermal transport behavior, corroborating our atomistic calculations in unveiling the role of molecular chain length and functional group. Molecular dynamics simulations reveal that the functionalization constrains the cross-plane scattering of low frequency phonons, which in turn enhances in-plane heat conduction of the bonded graphene film by recovering the long flexural phonon lifetime.

## INTRODUCTION

Anisotropic properties of two-dimensional (2D) layered materials make them promising in the application of next generation electronic device, among which graphene and few-layer graphene (FLG) have been most intensively studied for thermal management, due to their extraordinarily high in-plane thermal conductivity ( $\kappa$ ) [1–5]. For instance, Z. Yan et al. [6] reported that the maximum hotspot temperature can be lowered by  $\sim 20^\circ\text{C}$  in transistors operating at  $\sim 13\text{ W mm}^{-1}$  using FLG as a heat spreader for a gallium nitride (GaN) transistor. Gao et al. [7] reported that the maximum hotspot temperature decreased from  $121$  to  $108^\circ\text{C}$  ( $\Delta T = 13^\circ\text{C}$ ) for a heat flux of  $430\text{ W cm}^{-2}$  after the introduction of a single layer graphene (SLG) heat spreader. Moreover, the simulations of graphene heat spreaders were also reported for Silicon-on-Insulator (SOI) integrated circuits [8] and 3-D integrated circuits [9]. The thermal conductivity of graphene laminate film supported on substrate was also investigated and found to remain rather large [10]. However, in most practical applications, graphene/FLG will be supported by and integrated with insulators, both in an electronic circuitry and heat-spreader applications [11]. Therefore, thermal energy flow will be limited both by the in-plane thermal conductivity ( $\kappa$ ) of the supported graphene/FLG and by the thermal boundary resistance ( $R$ ) at the graphene/FLG-substrate interface [12].

Due to their exceedingly large surface-to-volume ratio, the properties of 2D layered materials are very sensitive to the interactions with external bodies. Indeed, when supported on an amorphous substrate,  $\kappa$  of suspended graphene decreased by almost one order of magnitude, from  $\sim 4000\text{ Wm}^{-1}\text{K}^{-1}$  [13] to  $\sim 600\text{ Wm}^{-1}\text{K}^{-1}$  [14]. Such a striking discrepancy in  $\kappa$  significantly limits the thermal performance of graphene/FLG in real applications. It is reported that the different behaviors are due to the strong scattering of the important heat carrying flexural acoustic (ZA) modes [15] to the substrate [16]. More specifically, it was identified that the phonon relaxation times (RTs) of graphene ZA modes are suppressed when supported on a  $\text{SiO}_2$  substrate. These studies have improved our fundamental understanding in the physics behind the problem and it was suggested that making rational choice of the substrate material [14] and modulating its coupling to graphene [12] may be useful to improve  $\kappa$  of the supported graphene/FLG.

The thermal boundary resistance ( $R$ ) of a graphene/FLG-substrate interface is another limiting factor to their thermal performance in devices. Covalent functionalization has

been proved to efficiently promote heat transfer between interfaces by introducing additional thermal pathways through the functionalizing molecules [17–32]. For example, self-assembled-monolayers (SAM) were used to functionalize metallic surfaces to enhance heat transport across metal-water [19, 26], metal-gas [27], metal-semiconductor [20] and metal-polymer [30] interface. Functionalization was used in graphene and CNT nanocomposites to mitigate the high thermal boundary resistance between the graphene/CNT fillers and the polymer matrices [17, 24, 25, 29]. Functionalized molecules also assist to align and densely pack multilayer graphene sheets and reduce the interlayer thermal resistance of graphene [24]. Recently, it was shown that plasma-functionalized graphene raised the cross-plane thermal conductance between aluminum and its substrate by a factor of two [18]. Nevertheless, the functionalization-introduced point defects will further decrease  $\kappa$  of the supported graphene/FLG, as they introduce phonons scattering centers [24, 31, 32].

To make progress, a robust solution that maintains the high thermal conductivity of graphene/FLG when supported, while effectively reducing the interface thermal resistance is needed. Here we demonstrate that thermal management of a micro heater is considerably improved via introducing alternative heat-spreading channels implemented with graphene-based film covalently bonded to functionalized graphene oxide through amino-silane molecules. We probed interface thermal resistance by photothermal reflectance measurements to demonstrate an improved thermal coupling due to functionalization on the graphene-graphene oxide interface and the graphene oxide-silica interface. Molecular dynamics simulations and ab initio calculations reveal that the functionalization constrains the cross-plane scattering of low frequency phonons, which in turn enhances in-plane heat conduction of the bonded graphene film by recovering the long flexural phonon lifetime. Our results provide evidence that a graphene film deposited on a functionalized graphene oxide substrate provides a very attractive platform for thermal management applications.

## RESULT AND DISCUSSION

A graphene-based film (GBF) bonded to the functionalized graphene oxide (FGO) substrate through silane molecules is shown in Figure 1(a) and (b). To synthesize experimentally GBF and FGO (figure 1c), we first prepared graphene oxide (GO) dispersion (See Experimental Section). The FGO was obtained by functionalizing GO with a silane-based

chemistry suitable for reactive oxide-forming surfaces including the basal plane of GO and SiO<sub>2</sub>. APTES has three -OCH<sub>2</sub>-CH<sub>3</sub> groups and one -NH<sub>2</sub> end, as shown in Fig. 1(a). Due to the simple chemistry and unique multi-functional nature of APTES, it can easily bind two different substrates. In our case, the -Si-O end of APTES binds to the graphene oxide substrate. -Si-OC<sub>2</sub>H<sub>5</sub> groups of APTES hydrolyse in water and form cross-link bonds with each other. The cross-linked Si-O structure acts as a strong bonding layer between the substrate and graphene-based films. On the other hand, the -NH<sub>2</sub> end of APTES binds onto carboxyl groups on the functionalized graphene film. The FGO layer has a thickness of  $\sim 5$  nm. The graphene film was fabricated from chemically reduced GO and can recover relatively high in-plane thermal conductivity after thermal annealing [33]. The graphene film was then spin-coated [34] with the FGO and the resulting bundle was transferred to a thermal evaluation device [7], resulting in the formation of molecular bridges between the graphene surface and the device's SiO<sub>2</sub> substrate. The thermal evaluation device was integrated with micro Pt-based heating resistors as the hot spot and temperature sensors [7], as shown in Fig. 1(d), acting as a simulation platform of an electronic component to demonstrate the heat-spreading capability of the supported graphene film. A direct current  $I$  was input into the circuit by applying an outer voltage  $V$  in Fig. 1(e), and hence the generated power is calculated as  $P = V \times I$ . Since the lateral dimension of the hotspot ( $A = 400 \times 400 \mu\text{m}^2$ ) is much larger than its thickness (260 nm), most of the heat is dissipated through the lateral direction of the hotspot. Hence the heat flux is defined as  $Q = P/A$ , and the direction is parallel to the substrate. The calibration relationship between the resistance  $R$  ( $\Omega$ ) and the temperature  $T$  ( $^{\circ}\text{C}$ ) of the thermal evaluation chip is  $R(T) = 0.21T + 112$ . The temperature measurement uncertainty is  $\epsilon = \pm 0.5^{\circ}\text{C}$ .

Figure 1(c) shows the temperature measured *in situ* at the hot spot and compares the thermal performance of the graphene-film with and without the functionalization. With a constant heat flux of  $1300 \text{ W cm}^{-2}$  at the Pt chip, the hotspot temperature decreased from  $135 \pm 0.5^{\circ}\text{C}$  to  $118 \pm 0.5^{\circ}\text{C}$  ( $\Delta T = 17 \pm 1^{\circ}\text{C}$ ) with a graphene-based film deposited on non-functionalized graphene oxide compared to the case of a bare chip. Such a remarkable temperature drop is far beyond the measurement uncertainty  $\Delta T \gg \epsilon$ . Furthermore, with the same heat flux input, the hotspot temperature further decreased from  $118 \pm 0.5^{\circ}\text{C}$  to  $112 \pm 0.5^{\circ}\text{C}$  ( $\Delta T = 6 \pm 1^{\circ}\text{C}$ ) thanks to the presence of the APTES functionalization. The heat-spreading performance is thus enhanced by  $\sim 35\%$  via the functionalization. We have

implemented a finite-element (FEM) model (See [35]) of the heat spreading device by taking the results of atomistic simulation as input parameters. As shown in Fig. 1(c), the heat-spreading performance of the equivalent macroscopic FEM model agrees reasonably well with the one measured by experiments.

To further confirm the enhanced heat spreading assisted by molecular functionalization, we measured the interface thermal resistance by using the pulsed photothermal reflectance (PPR) method [36, 37]. To enhance heat absorption, a gold layer is evaporated on the surface of the GO and FGO layers after dip coating. The sample is first excited by a Nd:YAG laser pulse. This causes a fast rise in the surface temperature followed by a relaxation. The change of surface temperature is monitored by a probe laser which reflects off from the samples' surface. Since the relaxation time is governed by the thermal properties of the underlying layers and interfacial thermal resistance between the layers, by obtaining the temperature profile one can extract the thermal properties of the layers and interface thermal resistance between the layers through a heat conduction model. Four sets of samples were fabricated, as shown in Fig. 2 and the thermal resistance  $R_1$  between the Au-Cr film and the (functionalized) graphene oxide layer, and the resistance  $R_2$  between (functionalized) graphene oxide layer and graphene-based film or SiO<sub>2</sub> were measured. The experimental setup and the procedure of thermal resistance extraction by fitting the photothermal response to the model (see Section I in [35]). The normalized surface temperatures of the four sample sets are shown in Fig. 2 and the extracted thermal resistances are reported in Table. I. A four-fold reduction is achieved in the thermal resistance between GO and GBF from  $3.8 \times 10^{-8}$  m<sup>2</sup>K/W to  $0.9 \times 10^{-8}$  m<sup>2</sup>K/W. On the GO-SiO<sub>2</sub> interface, the functionalization remarkably reduced the thermal resistance by a factor of almost three, from  $7.5 \times 10^{-8}$  m<sup>2</sup>K/W to  $2.6 \times 10^{-8}$  m<sup>2</sup>K/W. We also observe a better thermal coupling on the metal-dielectric interface between Au-Cr and GO due to the surface chemistry.

To gain a deeper insight into the impact of molecular structure on the thermal transport along the molecules, we used 3-Amino-propyltriethoxysilane (APTES), 11-Amino- undecyltriethoxysilane and 3-(Azidopropyl)-triethoxysilane as different functional agents on the graphene oxide to evaluate their heat spreading performance on the same thermal test platform. The same concentration of 0.1492 mol/kg is used for all three types of molecules. Fig. 3 shows the temperature reduction of the hot spot covered by graphene-based films with functionalized GO using three different molecules. The results show that the heat spreader

Interface	$R_1$ (m <sup>2</sup> K/W)	$R_2$ (m <sup>2</sup> K/W)
Au-Cr/GO/GBF	2.0E-8	3.8E-8
Au-Cr/FGO/GBF	1.1E-8	0.9E-8
Au-Cr/GO/SiO <sub>2</sub>	2.1E-8	7.5E-8
Au-Cr/FGO/SiO <sub>2</sub>	1.3E-8	2.6E-8

TABLE I. Au/(F-)GO and (F-)GO/X Interface thermal resistances. X = GBF or SiO<sub>2</sub>.

of GO functionalized with APTES has the best cooling performance. To properly understand this difference, an exploration of the internal vibrational properties of the molecule is crucial [38]. We hence investigated how the differences in the phonon transmission impact the interfacial thermal transport. In this aim, we probed the phonon transmission  $\Xi(E_{\text{ph}})$  by atomistic Green's Function (AGF) to characterize the local heat conduction with and without the presence of the molecule (Section V in [35]).  $\Xi(E_{\text{ph}})$  enables a precise measurement of the atomic-scale molecule-graphene heat transport that the conventional models fail to provide. The phonon transmission functions through different molecules and the associated thermal conductances versus temperature are shown in Fig. 3(b) and (c). The phonon transmission at low phonon energies across the 11-Aminoundecyltriethoxysilane molecule is comparable to that across the APTES molecule, whereas at high phonon energies ( $>4$  meV), the phonon transmission is considerably suppressed. Such a distinct phonon transport behavior is determined by the molecule chain length. By comparing the chemical structures, we can see that 11-Aminoundecyltriethoxysilane (-N-C<sub>11</sub>-Si-O<sub>3</sub>) has the same functional groups as APTES (-N-C<sub>3</sub>-Si-O<sub>3</sub>) but has a longer carbon backbone. Such a long chain length has a rather weak impact on the low frequency phonons due to their very long wavelength but can strongly suppress the phonon transport at high frequencies. On the other hand, when comparing the phonon transmission through the junction of APTES and 3-(Azidopropyl)triethoxysilane (-N<sup>-</sup>-N<sup>+</sup>-N-C<sub>3</sub>-Si-O<sub>3</sub>), it is evident to identify a stronger transmission at all frequencies. By comparing the chemical structures in Fig. 3(a), we can see that 3-(Azidopropyl)triethoxysilane has the same carbon backbone as APTES but has the -NN<sup>+</sup>N<sup>-</sup> group instead of an amino group. Such a functional group couples to the substrate through non-bonded van der Waals (vdW) interactions and thus has a much weaker thermal coupling than the amino group which is covalently functionalized to graphene ox-

ide. Given the same backbone structure, the phonon eigenmodes in the molecule have not been altered but the transmission is suppressed due to the weaker thermal coupling to the graphene reservoirs.

We now investigate the detailed vibrational and electronic transport properties of the APTES molecule since it presents the best performance in heat spreading. We probed the phonon transmission  $\Xi(E_{\text{ph}})$  to characterize the local heat conduction with and without the presence of the APTES molecule. As shown in Figure 4, the transmission function  $\Xi(E_{\text{ph}})$  for the two adjacent graphene layers without any molecule displays a clear stepwise structure that provides the number of phonon channels. Low energy phonons ( $E_{\text{ph}} \leq 10$  meV) dominate heat conduction since the adjacent graphene flakes interact only through weak vdW forces that inhibit the transmission of high-frequency phonons [39]. When the graphene layers are bridged by a amino-silane molecule, the high-frequency phonons act as the major contributors in the heat conductance  $G_{\text{ph}}$ , creating more phonon channels through the covalent bond vibrations. This is in line with the transmission calculation of Segal *et al.* [40] who observed a contribution to heat conduction by higher-frequency phonons within the molecule coupled to the low-frequency phonons responsible for heat transport in the thermal reservoirs. The oscillations in the transmission spectrum may originate from phonon interferences within the alkane chain [41–43]. Fabry-Pérot (FP) like interference effect occurs in the frequency region of  $E_{\text{ph}} = 20 - 100$  meV, as was previously observed in an alkane SAM interface [41]. Such FP like interferences originate from the multiple reflected phonons interfering constructively within the alkane chain, as the local maxima in the transmission (Figure 4) through the molecule can attain the same intensity of that through pristine graphene films at given frequencies. Although destructive quantum interference was believed unlikely to occur in a linear alkane chain [42], we observe strong destructive interference patterns in the high frequency range ( $\omega/2\pi = 40 - 60$  THz), which may correspond to two-path destructive phonon interferences [43, 44].

We investigated the inter-layer electron transport in the graphene and the effect of the silane intercalation in such a hybrid nanostructure through a *ab initio* calculation combined with Green’s function (Methods). As shown in Fig. 4(c) and (d), the presence of the molecule reduces the electron transmission by interrupting the  $\pi - \pi$  stacking of the phenyl rings in the adjacent graphene flakes. This means that the silane molecule eliminates the electrical current leakage by isolating the graphene heat spreader and the electronic device. Conse-

quently, the main heat carrier in this system is phonon as the thermal conductance due to the electron contributes to the total thermal conductance by  $\sim 4\%$  at room temperature with functionalization and by  $\sim 2\%$  without molecules.

To explore the effect of functional APTES molecules on the in-plane thermal conductance of the graphene film, we first perform molecular dynamic (MD) simulations to study a nanoscale molecular junction between two stacks of multi-layer graphene nanoflakes. For a weak oxidation, the thermal resistance of the graphene film and its oxidized substrate on one hand, and on the other hand its thermal conductivity are very close to those with a non-oxidized graphene support. The dependence of thermal resistance and conductivity of graphene film to the oxidation rate of the graphene oxide substrate is reported in [35].

We consider defect-free and isotopically pure graphene flakes of  $10 \times 10 \text{ nm}^2$  thermalized at 300 K (See methods and Section VI in [35]). The FGO substrate has a 5 nm thickness as in the experiments. Conventional silica substrate results in a substantial decrease of the basal-plane thermal conductivity of graphene due to the non-conformality of the substrate-graphene interface [14]. To compare, the FGO substrate proposed herein minimize the perturbation of substrate on the morphology of graphene (see Fig. 1(c)), thus maintaining its high thermal conductivity. Periodic boundary conditions were used in the in-plane directions so that the MD system corresponds to two thin films connected through silane molecules with the number density  $\rho$ , defined as the molecule number per graphene unit area.

To illustrate the intriguing role of the functionalizing molecule, the in-plane thermal conductivity  $\kappa$  of the film and its interfacial thermal resistance  $R$  (Section IV in [35]) with the FGO substrate is plotted as a function of the graphene layer number  $l_G$  in the film in Figure 5 (a) and (b), respectively. First a supercell containing a single molecule is studied, which corresponds to  $\rho = 0.081 \text{ nm}^{-2}$ . For  $l_G \geq 2$ , the presence of the APTES molecule results in an unexpected increase both in the graphene film thermal conductivity  $\kappa$  and in  $R$ . An overall decaying trend of the in-plane thermal conductivity  $\kappa$  of the graphene film and its resistance  $R$  with the substrate versus the layer number  $l_G$  is observed until approaching the value of bulk graphite. This is due to the increased cross-plane coupling of the low-energy phonons. A similar decay was found both in experimental measurements of  $\kappa$  [13] of suspended graphene and in simulation-based estimation of  $R$  [45]. Unlike silica-supported graphene [14], the few-layer graphene on functionalized graphene oxide support recovers the high thermal conductivity and follow the same decaying trend versus  $l_G$  as

the suspended graphene [13]. Therefore the proposed FGO substrate better conserves the high thermal conductivity of graphene compared to the silica substrate. Interestingly, for  $l_G = 1$ , the presence of the molecule reduces  $\kappa$ , which goes against the case where no molecule interconnects the graphene film and the substrate. This breakdown of the thermal conductivity enhancement is due to a saddle-like surface generated around the molecule's chemical bonds of amino and silano groups connecting the graphene, with the bond center as the saddle point, as shown in the inset A of Figure 5 (a). The saddlelike surface strongly scatters all phonon modes, thus decreasing  $\kappa$  of the graphene film. Such a curved surface was found quite common in defective graphene [46, 47], resulting from the Jahn-Teller effect to lower the energy by geometrical distortion [48]. The thermal conductance of a single silane molecule is determined to be 82 pW K<sup>-1</sup> through the molecular footprint (Section XI in [35]). Our simulated result is comparable to recent measurements of the thermal conductance of alkane thiols SAM at a silica-gold interface [38].

It is clearly seen from Fig. 5(a) that the critical layer number for the in-plane thermal conductivity switch is  $l_c = 2$ . This critical number depends on the level of conformation distortion of the functionalized graphene sheet. Several factors can play a role (see also Suppl. Mater. [35]): i) Molecule density. A diluted molecule distribution creates segregated ripples on the functionalized graphene sheet and even on the sheets further above thus interrupting the phonon mean free path. In this case more graphene sheets are required to recover the flat conformation, i.e.  $l_c > 2$ . For a high molecule density, the ripples tend to merge with themselves, recovering the flat surface in an extended area. Such merging hence recovers the interrupted phonon MFP and alleviates the detrimental influence of the separate ripples on the basal-plane thermal conductivity of graphene. In this case the two layers of graphene with functionalization have higher basal-plane thermal conductivity compared to that without functionalization, i.e.  $l_c = 2$ . ii) Functional group of the molecule. When the functional agent forms a stronger bond with its substrate than that of the amino-silane molecule, more severe static graphene distortion occurs thus increasing the critical number  $l_c$ . iii) Substrate of the graphene film. A highly mismatched substrate yields remarkable surface distortion of the graphene sheets in such a way that two layers of graphene are not sufficient to recover the high basal-plane thermal conductivity.

We investigate the microscopic origin of the thermal conductivity  $\kappa$  enhancement in the graphene film by probing the mode-wise phonon relaxation time (RT). The phonon RT  $\tau$

measures the temporal response of a perturbed phonon mode to relax back to equilibrium due to the net effect of different phonon scattering mechanisms.  $\tau$  can be defined as [49]  $\partial n / \partial \tau = (n - n_0) / \tau$  where  $n$  and  $n_0$  are the phonon occupation numbers out of and at thermal equilibrium. Under the single-mode-relaxation-time approximation, the thermal conductivity is given by  $\kappa = \sum_i C_i v_i^2 \tau_i$  where  $C_i$  and  $v_i$  are the specific heat per volume unit and the group velocity of the  $i$ -th phonon mode. The phonon dispersion of the supported graphene film for  $\rho = 0.081 \text{ nm}^{-2}$  and  $l_G=2$  and the extracted RT  $\tau$  for all the phonon modes are shown in Figure 6. By inserting the APTES molecule, the RT of the acoustic flexural modes  $\tau_{ZA}$  largely increase at low frequencies ( $\omega < 10 \text{ THz}$ ) whereas the longitudinal and transverse modes undergo a slight decrease in  $\tau_{LA,LO,TA,TO}$ . The notable increase in  $\tau_{ZA}$  accounts for the enhancement in  $\kappa$  of the graphene film bonded to the substrate since the ZA modes contribute considerably to  $\kappa$  as much as 77% at 300 K [15]. We attribute the increase in  $\tau_{ZA}$  to the weakened coupling between the graphene film and the substrate, which is reflected as the increased thermal resistance  $R$  for  $\rho = 0.081 \text{ nm}^{-2}$  and  $l_G \geq 2$ , as is shown in Fig. 5(b). An approximate expression from the perturbation theory for the RT due to phonon leakage towards the contact interface yields  $\tau^{-1} \propto g(\omega)K^2/\omega^2$ , where  $g(\omega)$  depends on the phonon density of states and  $K$  is the average vdW coupling constant between the graphene film and its substrate. A previous calculation [16] shows that  $K_{ZA}$  largely depends on the substrate morphology. The presence of the molecule strongly decreases the film-substrate coupling  $K_{ZA}$ , thus yielding a longer time  $\tau_{ZA}$ . This demonstrates that the amino-silane molecules refrain the film-substrate phonon scattering, which in turn enhances in-plane heat conduction in the bonded graphene film. Note that ZA mode becomes “massive” as shown in Fig. 6(a), i.e., the ZA branch does not reach all the way to zero frequency but shifts to higher frequencies. **The reduced inter-plane scattering compensates the reduction in the phonon group velocity at Brillouin zone center, so that the in-plane thermal conductivity increases after all (Section VIII in [35]).**

The cross-plane heat conduction between the top graphene films and the lower functionalized graphene oxide layers is governed by the competing effects of i) the intercalation of the molecules that tends to weaken the inter-layer coupling of graphene therefore increasing the cross-plane thermal resistance, ii) the additional heat channels introduced by the molecules covalently bonding the graphene sheets that tend to facilitate the cross-plane thermal coupling. We investigated the in-plane thermal conductivity  $\kappa$  of the graphene film

and its thermal resistance  $R$  with the functionalized substrate versus the equivalent APTES molecule number density  $\rho$  in Fig. 7. At a low molecule density, the molecule population is too small that the additional thermal phonon transport through the molecules cannot compensate the weakened cross-plane thermal coupling through the inter-layer vdW interactions due to the intercalation effect by the molecules. Therefore, the net effect is an increase in the cross-plane thermal resistance between the top graphene films and the lower graphene oxide layers compared to the non-functionalization case. In the limit of small number density, we consider the molecules as independent heat conductors connecting the film and the substrate.  $R$  agrees well with a reduced-model of parallel thermal resistors. Thus  $R$  decreases with the number of molecules.  $\kappa$  also decreases with the molecule number since the molecules increase the cross-plane phonon scattering in the graphene film. For larger  $\rho$ , the interactions among the molecules gain importance and  $R$  starts to deviate from the prediction of the parallel-thermal-resistor model, as shown in Fig. 7. the molecule population is large enough so that the additional thermal phonon transport through the molecules becomes very strong and compensates the weakened cross-plane thermal coupling through the inter-layer interactions due to the intercalation effect by the molecules. Therefore, the net effect is that the cross-plane thermal resistance between the top graphene films and the lower functionalized graphene oxide layers falls lower than that of the case without functionalization in the graphene oxide. For large  $\rho$ , the thermal resistance  $R$  is lower than that without molecules. However  $\kappa$  remains enhanced by a factor of  $\sim 15\%$  compared to its value for the non-functionalized graphene substrate. The molecule density  $\rho$  effectively tunes the thermal conductivity of the supported graphene.

## CONCLUSIONS

We demonstrate experimentally that thermal management of a micro heater is substantially improved via introducing alternative heat-escaping channels implemented with graphene-based film covalently bonded to functionalized graphene oxide through amino-silane molecules. Pulsed photothermal reflectance measurements of the interface thermal resistance demonstrated that the functionalization facilitates the interfacial phonon transport on the graphene-graphene oxide interface. Three functionalization polymers manifest distinct interfacial thermal transport behavior in the experiments, corroborating our atomistic

calculations in unveiling the intriguing role of molecular chain length and the functional group. Atomistic calculations show that the functionalization constrains the cross-plane scattering of low frequency phonons, which in turn enhances in-plane heat conduction of the bonded graphene film through phonon lifetime prolongation. Molecular dynamics simulation results show a flexible tuning of the in-plane thermal conductivity of the supported graphene by adjusting the molecule density. Our atomistic calculations provide a microscopic insight and disclose the physics of phonon transport between two graphitic nanomaterials bonded with molecules. Such a strategy is experimentally proven to be viable and important to the engineering of graphene electronics with improved heat transfer properties.

## METHODS

*Experimental method.* (i) Sample Synthesis. Graphite (Sigma, 4g),  $\text{H}_2\text{SO}_4$  (92 mL, 98%),  $\text{NaNO}_3$  (2g) and  $\text{KMnO}_4$  (12g) was used to prepare graphene oxide (GO) dispersion by following Hummers Method [50]. The obtained GO dispersion was reduced by L-ascorbic acid (LAA), polyvinyl alcohol (PVA) was also added for better suspension. The graphene-based film was prepared via vacuum filtration with polycarbonate filter paper with the pore size of 3  $\mu\text{m}$ . The film thickness was controlled by the filtration volume and the graphene concentration in the suspension. After dissolving the filter paper in pure acetone, a freestanding graphene-based film was obtained. The thickness of the graphene-based film was measured as approximately 20  $\mu\text{m}$ . Raman spectroscopy data of the GBF before and after the spin-coating with FGO is shown in Supporting Information Section II [35]. (ii) Functionalization. GO powder (20 mg) and Dicyclohexylcarbodiimide (DCC) (5 mg) were mixed with (3-Aminopropyl) triethoxysilane (APTES) (30 mL) by ultrasonication for 2h to produce a homogeneous suspension. Then the suspension was heated up to 100°C for 3h with continuous stirring to realize the functionalization. Fourier Transform Infrared Spectroscopy (FTIR) data provides evidence for the functionalization (Section III in [35]). (iii) Transfer process. The graphene-based film was first transferred onto a thermal release tape, and then spin-coated [34] with the FGO layer at 4000 rpm for 2 min onto the film. The thermal release tape was removed by heating the device.

*Simulation setup.* classical MD simulations were performed using LAMMPS [51]. Adaptive intermolecular reactive empirical bond order (AIREBO) potential [52] was used to simulate

the graphene's C-C interactions. The intramolecular forces are taken into account through the ReaxFF potential [53] which uses distance-dependent bond-order functions to represent the contributions of chemical bonding to the potential energy. Periodic boundary conditions are applied in the in-plane directions and free boundary condition in the cross-plane direction of the graphene system. First, each super cell was relaxed at the simulation temperature to achieve zero in-plane stress. Then the systems were thermalized by using a Langevin heat bath. After the thermalization, MD runs with durations equal to 600 picoseconds with a timestep of 0.2 femtosecond were carried out in the microcanonical ensemble to sample the temperature and heat flux to be used in the calculation of the thermal resistance and thermal conductivity. Calculation details concerning the thermal resistance, thermal conductivity, phonon transmission and phonon relaxation time can be found in the Supporting Information [35].

*Ab initio* calculations were carried out using the quantum chemistry DFT code SIESTA [55]. All systems were first geometrically optimized in isolation, with a generalized local-density approximations (LDA) within Ceperley-Alder version (CA), double-zeta polarized basis set, 0.01 eV/Å force tolerance and 250 Ry mesh cutoff. The relaxed atomic structures can be seen in Supplemental Figures. Electron transmission coefficients were computed using the GOLLUM [56] code. To produce the conductance curves in Fig. (4), the transmission coefficient  $T_{\text{el}}(E_F)$  was calculated for each relaxed junction geometry, by first obtaining the corresponding Hamiltonian and then overlapping matrices with SIESTA and double-zeta polarized basis set. To produce conductance-trace curves, the transmission coefficient  $T_{\text{el}}(E_F)$  was calculated for each relaxed junction geometry and the conductance  $G_{\text{el}}/G_0 = T_{\text{el}}(E_F)$  was obtained by evaluating  $T_{\text{el}}(E_F)$  at the Fermi energy  $E_F$ .

*Thermal conductance* Thermal conductance  $\kappa = \kappa_e + \kappa_{ph}$  where  $\kappa_{ph}$  ( $\kappa_e$ ) is the thermal conductance due to the phonons (electrons). From the Phonon transmission  $\Xi(E_{\text{ph}})$  the thermal conductance due to the the phonon could be calculated as  $\kappa_{ph}(T) = \int_0^\infty d\omega \left(-\frac{\partial f_{\text{BE}}}{\partial E}\right) \hbar\omega\Xi(\omega)/2\pi$ . where  $\omega$  is the frequency.  $T$  refers to the mean temperature of the system,  $f_{\text{BE}}$  is the Bose-Einstein phonon statistics.  $k_B$  and  $\hbar$  represent the Boltzmann and the reduced Plancks constants, respectively. The thermal conductance due to the electrons [54] could be calculated from the electron transmission coefficient  $T_{\text{el}}$  as  $\kappa_e(T) = \frac{L_0 L_2 - L_1^2}{\hbar T L_0}$  where  $L_n = \int_{-\infty}^\infty dE (E - E_F)^n T_{\text{el}}(E) \left(-\frac{\partial f_{\text{FD}}}{\partial E}\right)$  where  $f_{\text{FD}}$  is the Fermi-Dirac electron statistics.

## ACKNOWLEDGEMENT

This work was supported by the NANOTHERM project co-funded by the European Commission under the “Information and Communication Technologies” Seven Framework Program (FP7) and the Grant Agreement No. 318117. This work is also supported by the UK EPSRC, EP/K001507/1, EP/J014753/1, EP/H035818/1, and from the EU ITN MOLESCO 606728.

---

\* haoxue.han@ecp.fr

† c.lambert@lancaster.ac.uk

‡ johan.liu@chalmers.se

§ sebastian.volz@ecp.fr

- [1] Z Yan, DL Nika, AA Balandin, *IET Circuits, Devices and Systems*, **9**, 4 (2015).
- [2] A. K. Geim and K. S. Novoselov, *Nat. Mater.* **6**, 183 (2007).
- [3] A. A. Balandin, S. Ghosh, W. Z. Bao, I. Calizo, D. Teweldebrhan, F. Miao, and C. N. Lau, *Nano Lett.* **8**, 902 (2008).
- [4] A. A. Balandin. Thermal properties of graphene and nanostructured carbon materials. *Nat. Mater.* **10**, 569 (2011).
- [5] Q.-Q. Kong, Z. Liu J.-G. Gao, C.-M. Chen, Q. Zhang, G. Zhou, Z.-C. Tao, X.-H. Zhang, M.-Z. Wang, F. Li and R. Cai. Hierarchical GrapheneCarbon Fiber Composite Paper as a Flexible Lateral Heat Spreader. *Adv. Func. Mater.* **24**, 4222 (2014)
- [6] Z. Yan, G. Liu, J. M. Khan, and A. A. Balandin, Graphene quilts for thermal management of high-power GaN transistors, *Nature Communications*, vol. 3, p. 827, 2012.
- [7] Z. Gao, Y. Zhang, Y. Fu, M. M. F. Yuen, and J. Liu, Thermal chemical vapor deposition grown graphene heat spreader for thermal management of hot spots, *Carbon*, vol. 61, pp. 342-348, 2013.
- [8] S. Subrina, D. Kotchetkov, and A. A. Balandin, Heat Removal in Silicon-on-Insulator Integrated Circuits With Graphene Lateral Heat Spreaders, *IEEE Electron Device Letters*, vol. 30, pp. 1281-1283, Dec 2009.

- [9] S. Subrina, Modeling Based Design of Graphene Heat Spreaders and Interconnects in 3-D Integrated Circuits, *Journal of Nanoelectronics and Optoelectronics*, vol. 5, pp. 281-286, Dec 2010.
- [10] H. Malekpour, et al., *Nano Letters*, 14, 5155 (2014).
- [11] R. Prasher. Graphene Spreads the Heat. *Science*, **328**,(5979), 185-186 (2010)
- [12] Zhun-Yong Ong and Eric Pop. Effect of substrate modes on thermal transport in supported graphene. *Phys. Rev. B* **84**, 075471 (2011).
- [13] S. Ghosh, W. Z. Bao, D. L. Nika, S. Subrina, E. P. Pokatilov, C. N. Lau, and A. A. Balandin. *Nat. Mater.* **9**,(7) 555 (2010).
- [14] M. M. Sadeghia, I. Joa, and L. Shi. Phonon-interface scattering in multilayer graphene on an amorphous support. *Proc. Natl. Acad. Sci. U.S.A.* **110**,(41) 16321 (2013).
- [15] L. Lindsay, D. A. Broido, and N. Mingo, Flexual phonons and thermal transport in graphene. *Phys. Rev. B* **82**, 115427 (2010).
- [16] J.H. Seol, I Jo, A.L. Moore, L. Lindsay, Z.H. Aitken, M.T. Pettes MT, et al. Two-dimensional phonon transport in supported graphene. *Science* **328**, 213 (2010).
- [17] T. Luo and J. R. Lloyd. Enhancement of Thermal Energy Transport Across Graphene/Graphite and Polymer Interfaces: A Molecular Dynamics Study. *Adv. Mater.* **22**, 2495 (2012)
- [18] P. E. Hopkins, M. Baraket, E. V. Barnat, T. E. Beechem, S. P. Kearney, J. C. Duda, J. T. Robinson, S. G. Walton, Manipulating Thermal Conductance at Metal-Graphene Contacts via Chemical Functionalization. *Nano Lett.* **12**, 590 (2012).
- [19] Z. Ge, D. G. Cahill, and P. V. Braun. Thermal Conductance of Hydrophilic and Hydrophobic Interfaces. *Phys. Rev. Lett.* **96**, 186101 (2006)
- [20] R. Y. Wang, R. A. Segalman and A. Majumdar. Room temperature thermal conductance of alkanedithiol self-assembled monolayers. *Appl. Phys. Lett.* **89**, 173113 (2006).
- [21] T. Ramanathan, A. A. Abdala, S. Stankovich, D. A. Dikin, M. Herrera-Alonso, R. D. Piner, D. H. Adamson, H. C. Schniepp, X. Chen, R. S. Ruoff, S. T. Nguyen, I. A. Aksay, R. K. Prud'Homme and L. C. Brinson. Functionalized graphene sheets for polymer nanocomposites. *Nat Nanotechnol* **3**, 327-331 (2008).
- [22] D. Konatham and A. Striolo. Thermal boundary resistance at the graphene-oil interface. *Appl. Phys. Lett.* **95**, 163105 (2009).

- [23] K. C. Collins, S. Chen, G. Chen. Effects of surface chemistry on thermal conductance at aluminum-diamond interfaces. *Appl. Phys. Lett.* **97**, 083102 (2010).
- [24] Q. Liang, X. Yao, W. Wang, Y. Liu, and C. P. Wong. A Three-Dimensional Vertically Aligned Functionalized Multilayer Graphene Architecture: An Approach for Graphene-Based Thermal Interfacial Materials. *ACS Nano*, **5**(3), 2392-2401 (2011).
- [25] Y. Ni, H. L. Khanh, Y. Chalopin, J. Bai, P. Lebarney, L. Divay and S. Volz. Highly efficient thermal glue for carbon nanotubes based on azide polymers. *Appl. Phys. Lett.* **100**, 193118 (2012).
- [26] H. Harikrishna, W. A. Ducker and S. T. Huxtable. The influence of interface bonding on thermal transport through solid-liquid interfaces. *Appl. Phys. Lett.* **102**, 251606 (2013).
- [27] Z. Liang, W. Evans, T. Desai and P. Keblinski. Improvement of heat transfer efficiency at solid-gas interfaces by self-assembled monolayers. *Appl. Phys. Lett.* **102**, 061907 (2013).
- [28] P. J. O'Brien, S. Shenogin, J. Liu, P. K. Chow, D. Laurencin, P. H. Mutin, M. Yamaguchi, P. Keblinski and G. Ramanath. Bonding-induced thermal conductance enhancement at inorganic heterointerfaces using nanomolecular monolayers. *Nature Mater.* **12**, 118 (2013).
- [29] J. H. Taphouse, O'Neil L. Smith, S. R. Marder and B. A. Cola. A Pyrenylpropyl Phosphonic Acid Surface Modifier for Mitigating the Thermal Resistance of Carbon Nanotube Contacts. *Adv. Func. Mater.* **24**, 465 (2014)
- [30] F. Sun, T. Zhang, M. M. Jobbins, Z. Guo, X. Zhang, Z. Zheng, D. Tang, S. Ptasinska and T. Luo. Molecular Bridge Enables Anomalous Enhancement in Thermal Transport across Hard-Soft Material Interfaces. *Adv. Mater.* **26**, 6093 (2014)
- [31] S.-K. Chien, Y.-T. Yang and C.-K. Chen. Influence of hydrogen functionalization on thermal conductivity of graphene: Nonequilibrium molecular dynamics simulations. *Appl. Phys. Lett.* **98**, 033107 (2011).
- [32] J. Y. Kim, J.-H. Lee, and J. C. Grossman. Thermal Transport in Functionalized Graphene. *ACS Nano*, **6**(10), 9050-9057 (2012).
- [33] Xin, G., Sun, H., Hu, T., Fard, H. R., Sun, X., Koratkar, N., Borca-Tasciuc, T. and Lian, J. (2014), Large-Area Freestanding Graphene Paper for Superior Thermal Management. *Adv. Mater.*, **26**: 4521-4526.
- [34] R. M. Pasternack, S. R. Amy and Y. J. Chabal. *Langmuir* **24**, (22), 12963-12971 (2008)

- [35] See Supporting Information for Fourier Transform Infrared Spectroscopy data of the FGO, Raman spectroscopy data of the GBF before and after the spin-coating with FGO, calculation methods and simulation details of thermal resistance, thermal conductivity, phonon relaxation time and dispersion curves using equilibrium molecular dynamics, thermal conductance and phonon transmission calculations using atomistic Green's Function, electrical Transport properties from Ab initio calculations combined with Green's function and the Finite-Element modeling of the thermal evaluation platform.
- [36] Chen, G. and Hui, P. Pulsed photothermal modeling of composite samples based on transmission-line theory of heat conduction. *Thin Solid Films*, 339(1), 58-67. (1999)
- [37] Y. Zhao, C. Zhu, S. Wang, J. Z. Tian, D. J. Yang, C. K. Chen, H. Cheng and P. Hing, Pulsed photothermal reflectance measurement of the thermal conductivity of sputtered aluminum nitride thin films *J. Appl. Phys.* 96, 4563 (2004)
- [38] T. Meier, F. Menges, P. Nirmalraj, H. Hölscher, H. Riel,<sup>1</sup> and B. Gotsmann. Length-Dependent Thermal Transport along Molecular Chains. *Phys. Rev. Lett.* **113**, 060801 (2014).
- [39] Juekuan Yang, Meng Shen, Yang Yang, William J. Evans, Zhiyong Wei, Weiyu Chen, Alfred A. Zinn, Yunfei Chen, Ravi Prasher, Terry T. Xu, Pawel Keblinski, and Deyu Li. Phonon Transport through Point Contacts between Graphitic Nanomaterials. *Phys. Rev. Lett.* **112**, 205901 (2014).
- [40] D. Segal, A. Nitzan, and P. Hänggi, *J. Chem. Phys.* **119**, 6840 (2003).
- [41] L. Hu, L. Zhang, M. Hu, J. S. Wang, B. Li, and P. Keblinski, *Phys. Rev. B* **81**, 235427 (2010).
- [42] Troels Markussen. Phonon interference effects in molecular junctions. *J. Chem. Phys.* **139**, 244101 (2013).
- [43] Haoxue Han, Lyudmila G. Potyomina, Alexandre A. Darinskii, Sebastian Volz, and Yuriy A. Kosevich. Phonon interference and thermal conductance reduction in atomic-scale metamaterials. *Phys. Rev. B* **89**, 180301(R) (2014)
- [44] Haoxue Han, Baowen Li, Sebastian Volz, and Yuriy A. Kosevich. Ultracompact Interference Phonon Nanocapacitor for Storage and Lasing of Coherent Terahertz Lattice Waves. *Phys. Rev. Lett.* 114, 145501 (2015)
- [45] Y. Ni, Y. Chalopin, and S. Volz. Significant thickness dependence of the thermal resistance between few-layer graphenes. *Appl. Phys. Lett.* **103**, 061906 (2013).
- [46] M. T. Lusk and L. D. Carr, *Phys. Rev. Lett.* **100**, 175503 (2008).

- [47] J.-W. Jiang, B.-S. Wang and J.-S. Wang. First principle study of the thermal conductance in graphene nanoribbon with vacancy and substitutional silicon defects. *Appl. Phys. Lett.* **98**, 113114 (2011).
- [48] T. Hughbanks and R. Hoffmann, *J. Am. Chem. Soc.* **105**, 3528 (1983).
- [49] J. M. Ziman, *Electrons and Phonons* (Oxford University Press, London, 1960).
- [50] W. S. Hummers, R. E. Offeman. *Journal of the American Chemical Society* **80**(6), 1339-1339 (1958).
- [51] S. Plimpton, *J. Comput. Phys.* **117**, 1 (1995).
- [52] S. J. Stuart, A. B. Tutein, and J. A. Harrison, *J. Chem. Phys.* **112**, 6472 (2000).
- [53] Chenoweth, van Duin and Goddard, *Journal of Physical Chemistry A*, **112**, 1040-1053 (2008).
- [54] Hatef Sadeghi, Sara Sangtarash, and Colin Lambert. Enhancing the thermoelectric figure of merit in engineered graphene nanoribbons *Beilstein Journal of Nanotechnology* **6**, **1** 1176 (2015).
- [55] Soler, Jos M., et al. The SIESTA method for ab initio order-N materials simulation *Journal of Physics: Condensed Matter* **14**, **11** 2745 (2002).
- [56] J Ferrer, CJ Lambert, VM Garca-Surez, D Zs Manrique, D Visontai, L Oroszlany, R Rodriguez-Ferrads, I Grace, SWD Bailey, K Gillemot, Hatef Sadeghi, LA Algharagholy GOLLUM: a next-generation simulation tool for electron, thermal and spin transport *New Journal of Physics* **16**, **9** 093029 (2014).

FIG. 1. (a) Sketch of the chemical bonds of the silane molecule. (b) Schematic of a graphene film on different supports. Left: Conventional silica substrate. Right: the proposed silica / functionalized graphene oxide substrate. (c) Schematic of the measurement setup. The chip is embedded in the  $\text{SiO}_2$  substrate. T- $\text{SiO}_2$  stands for thermally-grown  $\text{SiO}_2$ . Scanning electron microscopy (SEM) image of the in-plane and the cross section of the GBF. (d) SEM image of the chip as the hotspot. The scale bar is  $100 \mu\text{m}$ . (e) Calibration relationship between the resistance  $R$  ( $\Omega$ ) and the temperature  $T$  ( $^\circ\text{C}$ ) of the thermal evaluation chip. The temperature measurement uncertainty is  $\pm 0.5^\circ\text{C}$ . (f) Measured (filled markers) and FEM simulated (lines) chip temperatures versus the in-plane heat fluxes dissipated in (rectangles) a bare hotspot, (circles) a hotspot covered by a GBF, (up triangle) a chip covered by a GBF with non-functionalized GO and (down triangle) a chip covered by a GBF with APTES functionalized GO.

FIG. 2. Normalized surface temperature of Pulsed Photothermal Reflectance (PPR) measurements of the thermal interface resistance for (a) Au-Cr/FGO/GBF and Au-Cr/GO/GBF samples and (b) Au-Cr/FGO/ $\text{SiO}_2$  and Au-Cr/GO/ $\text{SiO}_2$  samples. (inset) Sample geometry for the PPR measurement.  $R_1$  and  $R_2$  refer to the thermal interface resistance between the Au-Cr film and the (APTES functionalized) graphene oxide layer, and that between (functionalized) graphene oxide layer and graphene-based film or  $\text{SiO}_2$ . The thermal resistances are also reported in Table. I.

FIG. 3. Heat spreading performance of graphene-based film on functionalized graphene oxide with different functional polymers: 3-Aminopropyltriethoxysilane (APTES), 11-Aminoundecyltriethoxysilane and 3-(Azidopropyl)triethoxysilane. (a) Measured temperature drop of heat spreaders with different functionalization polymers compared with that with non-functionalized GO. (b) Phonon transmission function  $\Xi(E_{\text{ph}})$  for three different types of molecules used in the experiment. (c) Phonon thermal conductance through the molecules as a function of temperature. The coloration of the data curves in (b) and (c) is the same as in subfigure (a).

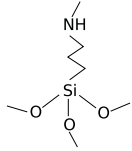
FIG. 4. (a) Phonon transmission  $\Xi(E_{\text{ph}})$  versus phonon energy  $E_{\text{ph}} = \hbar\omega$  (red curve) between two adjacent graphene layers and (blue curve) through the APTES molecule bonding the two graphene layers. (b) Thermal conductances  $G_{\text{th}} = G_e + G_{\text{ph}}$  contributed by phonons  $G_{\text{ph}}$  (solid lines) and by electrons  $G_e$  (dashed lines) versus temperature for the two cases. (c) Electron transmission  $T_{\text{el}} = G_{\text{el}}/G_0$  versus Fermi energy  $E_F$  between two adjacent graphene layers and (blue curve) through the APTES molecule bonding the two graphene layers. (d) Electronic thermal conductances  $\kappa_{\text{el}}(T)$  versus temperature for the two cases.

FIG. 5. (a) MD simulation results of in-plane thermal conductivity  $\kappa$  of the graphene film and (b) interfacial thermal resistance  $R$  between the FGO substrate and the graphene film versus the graphene layer number  $l_G$  in the film. The molecule density is  $\rho = 0.081 \text{ nm}^{-2}$ . Cases with (red circles) and without (blue squares) the APTES molecule are compared. The values of thermal conductivity are normalized to that of the single-layer graphene. Inset A illustrates a saddlelike surface generated by the APTES molecule for  $l_G = 1$ . Inset B shows that the saddlelike curvature disappears for  $l_G \geq 1$ . The measurements of suspended and supported graphene are from [13] and [14], respectively. The simulated (resp. measured) thermal conductivity is normalized with respect to that of the simulated (resp. measured) graphite to allow a reasonable comparison.

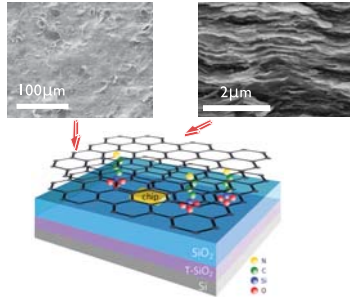
FIG. 6. (a) Phonon dispersion of the graphene film bonded to the APTES-FGO substrate from MD simulations, for  $\rho = 0.081 \text{ nm}^{-2}$  and  $l_G=2$ . (b), (c) and (d) Mode-wise phonon relaxation time for longitudinal modes including longitudinal acoustic (LA) and optical (LO) branches, for transverse modes including transverse acoustic (TA) and optical (TO) branches, and for flexural modes including flexural acoustic (ZA) and optical (ZO) branches, respectively. For low frequency phonons,  $\tau$  follows the  $\omega^{-2}$  scaling rule of the Umklapp processes at low frequency and high-temperature limits.

FIG. 7. Thermal conductivity  $\kappa$  (red circles) of the graphene film and its thermal resistance  $R$  (blue squares) with the APTES functionalized substrate versus the equivalent molecule number density  $\rho$ . (Green line) Resistance  $R_{rm}$  predicted by a reduced-model of parallel thermal resistors is to compare with the MD results for small  $\rho$ .  $R_{rm} = (1/R_0 + N/R_m)^{-1}$  where  $R_0$  is the thermal resistance between two adjacent graphene layers and  $R_m$  is the additional resistance induced by a single molecule. The values of  $R_0$  and  $R_m$  are determined in MD simulations:  $R_0 = 0.203 \text{ mm}^2\text{KW}^{-1}$  and  $R_m = 0.069 \text{ mm}^2\text{KW}^{-1}$ . Red and blue dashed lines represent, respectively,  $\kappa$  and  $R$  without the interconnecting molecule between at the film-substrate interface.

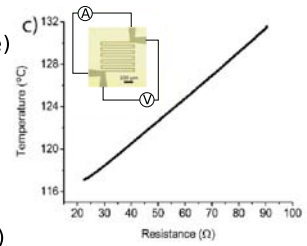
(a)



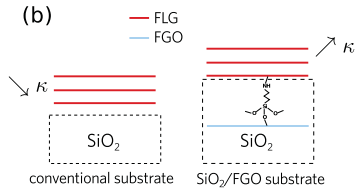
(c)



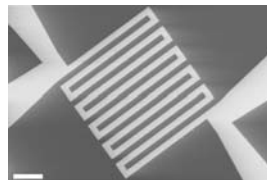
(e)



(b)



(d)



(f)

